



Review

A Literature Survey on Electrical-Current-Assisted Friction Stir Welding

Moosa Sajed ¹, John William Grimaldo Guerrero ² and Hamed Aghajani Derazkola ^{3,*}

¹ Department of Mechanical Engineering, Azarbaijan Shahid Madani University, Tabriz-Maragheh Road, Tabriz 53714-161, Iran

² Department of Energy, Universidad de la Costa, Barranquilla 080001, Colombia

³ Department of Mechanics, Design and Industrial Management, University of Deusto, Avda Universidades 24, 48007 Bilbao, Spain

* Correspondence: h.aghajani@deusto.es

Abstract: Electrical-current-assisted friction stir welding (EA-FSW) is a procedure developed for the joining of similar and dissimilar materials. EA-FSW is a newly invented solid-state process to increase welded components' efficacy in various applications, such as marine structures. EA-FSW joints have investigated the dissimilar joints on aluminum–magnesium, aluminum–steel, and polymer-to-steel. Similar joints have been performed on aluminum, magnesium, and steel. The main parameters that affect the temperature of the nugget in EA-FSW are electrical current and tool rotational velocity. This review paper presents the fundamental principle of EA-FSW, its processes mechanism, and various types of tools, and discusses the different joints that EA-FSW welded. The effect of electrical current on the quality of similar and dissimilar joints is discussed. The simulation process and detailed modeling of the EA-FSW process are discussed in the last section.

Keywords: electrical-assisted friction stir welding; similar joints; dissimilar joints; process parameters



Citation: Sajed, M.; Guerrero, J.W.G.; Derazkola, H.A. A Literature Survey on Electrical-Current-Assisted Friction Stir Welding. *Appl. Sci.* **2023**, *13*, 1563. <https://doi.org/10.3390/app13031563>

Academic Editor: Guijun Bi

Received: 22 November 2022

Revised: 22 January 2023

Accepted: 24 January 2023

Published: 25 January 2023



Copyright: © 2023 by the authors. Licensee MDPI, Basel, Switzerland. This article is an open access article distributed under the terms and conditions of the Creative Commons Attribution (CC BY) license (<https://creativecommons.org/licenses/by/4.0/>).

1. Introduction

Friction stir welding (FSW) is a solid-state joining process in development. This process was introduced by The Welding Institute (TWI) in 1991 for the similar joining of aluminum alloys [1]. In this technique, a hard-non-consumable tool rotates and penetrates the joint line [2]. The tool action is applied by a welding machine [3]. The welding machine exerts an axial force during the welding procedure, in order to be in touch with the workpieces [4]. Due to the presence of friction between the tool and welding materials, heat generates at the tool–workpiece interface [5]. This heat is the result of the sliding friction and deformation of the base metal [6]. Due to the available experimental test, the generated heat during the FSW process has not been increased above the base metals' melting points [7]. Although, in some cases, local melting was also reported for materials with a low melting point. The FSW process is also called a thermomechanical process, and this process has also been categorized in solid-state joining techniques [8]. FSW is developing rapidly, particularly in the application of hard-weldable materials such as aluminum alloys, magnesium alloys, zinc alloys, copper, and others that are not weldable or joined with specific welding processes [9]. The flexibility of the FSW process has allowed various dissimilar joints to be producible [10]. Research has shown that the joining of dissimilar metals, polymers, and even dissimilar joints between polymers and metals are reachable with the FSW process [11]. The advantages of the FSW process include low heat input, low changes in base materials after joining, no or little filler material, no fume and welding spatter, very little pre-processing before the joining procedure, less residual stress after joining, and lower levels of pores and cracks [12]. For these reasons, FSW has been rapidly used in various industries and has produced enormous amounts of economically efficient products [13]. FSW was utilized successfully for the joining of non-ferrous metals

at below the melting point [14]. Although, in the case of metals with a high melting point, using FSW faces some issues, such as choosing a tool material, tool wear, and energy consumption. The final joint's quality is related to the welded sample's ultimate tensile strength and hardness. The welding researchers try to achieve the highest ultimate tensile strength in the welded samples. The best properties belong to the weld with the lowest porosity and mechanical properties similar to higher weldments. The researchers found that the FSW process for joining high-melting-temperature materials or refractory metals such as ultra-high-strength steels, chromium alloys, Tantalum, and Tungsten alloys is not effective [15]. This means that, from the technical point of view, the tool wear during FSW is very high and cannot weld the raw materials. As a consequence, the final joint mechanical properties would be quite low. In some metals, such as Tantalum and Tungsten, it is not possible to conduct FSW because the tool should be more rigid with a higher strength than raw material. In this case, there is no report for FSW of Tantalum and Tungsten because these metals are used for FSW tools, not weldments [16,17].

There are various literature sources that demonstrate the researchers used extra-hard materials for the FSW tool, changed joint geometry, and used specific tool shapes in order to decrease defect possibility in the joint line after the FSW process [17]. All these factors have drawbacks, such as using expensive materials for producing the tool, the limitation of using various tool shapes with a high risk of breaking during welding, and undesirable joint geometry [18]. Research in this area has shown that FSW of high melting temperature or hard materials needs support, and development in the conventional FSW process can improve the final joint [19]. On the other hand, it was necessary to decrease extra expenses by changing the joint line geometry, using ultra-hard materials for the tool, and producing the FSW tool with specific profiles.

Recently, assisted friction stir welding processes, such as laser assist [20], ultrasonic assist [21], rapid cooling assist [19], fed friction stir welding [22], arc assist, and electrical-assisted friction stir welding have been introduced by various research groups to increase the efficacy of FSW for the joining of high-melting-temperature materials. The application of a laser resulted in lower residual stress [20]. It is reported that the application of ultrasonic vibrations has no impact when a low welding speed is used, while it is useful when a high-speed welding process is used [21]. Rapid cooling also affects almost all aspects of the joint, including grain size, microhardness, etc. [20]. Fed friction stir welding is a novel welding method used to join polymers to metals, where reinforcing particles are injected into the nugget during welding, which improves the mechanical properties of the joint [21]. In this paper, the details and advances of the electrical-current-assisted friction stir welding (EA-FSW) method will be discussed [23]. Electrical current assistance can help improve joint microstructure, increase the flow ability of base materials at dissimilar joints, and decrease the welding time to increase the process efficacy in industries.

2. Principle of EA-FSW Method

The EA-FSW is a developed process that is a combination of FSW and resistance welding. The EA-FSW, as a hybrid welding method, benefits from frictional heat and electrical current, and frictional heat plus resistance heat is used as the welding heat source for joining the workpieces. In EA-FSW, the workpieces are firmly placed to the joining fixture, in order to avoid their separation and any movements during the joining process. A rotational tool with a relatively thin pin is rotated and moved downward to insert it into the interface of the workpiece. Generally, the FSW tool is made of a hard material, and after penetration of the workpiece interface, the FSW tool moves forward along the joint line. Simultaneously, electrical current is provided, which flows between the FSW tool and the workpiece interface. In this stage, electrical resistance heat generates in the joint line and adds to the frictional heat produced by the rotational tool. The electrical resistance heats the joint line and is combined with frictional heat to soften and plasticize the workpieces.

The additional electrical current makes the workpieces softer and decreases the welding force. This phenomenon increased the traverse speeds of the welding force to build

a sound solid-state welding joint. This method can be implemented for the joining of ferrous and non-ferrous metals. Moreover, the hard materials can be joined much easier with this method. The FSW tool's working life increases by providing an additional heat source during the joining process. Higher welding quality and mechanical properties of final joints can be achieved at a shorter welding time. Due to the decreasing welding force, the joint line can be produced faster in EA-FSW. With extra electrical heating, the internal defects formation, such as wormholes and uncomplete mixing, is minimized. On the other hand, the residual stress of welded plates after EA-FSW is much lower than in the regular FSW process. This is due to the processing of material at elevated temperatures. The additional equipment needed to add the FSW process is simple, relatively cheap, and easy to use [24]. The electrical current is applied from a DC or AC power supply for the EA-FSW. The type of power supplier may be different in similar or dissimilar joints. The leads are fixed on the workpiece or welding tool for the passing electrical current, while insulating components, such as a ceramic plate, are fixed on the fixture or tool. The amount of current depends on the raw materials that are supposed to be welded. The electrical current would be greater for hard materials than for soft materials. Because a high current leads to overheating or melting of the raw materials, the used current range should be calculated according to electrical resistance properties. After that, the range of used electrical current should be calculated and considered for tests.

3. Various Types of EA-FSW

There are three main categories for the EA-FSW. The first category is called the preheating model in EA-FSW (Figure 1a), the second category is called the heat treatment model in EA-FSW (Figure 1b), and the last one is known as the combination model in EA-FSW (Figure 1c).

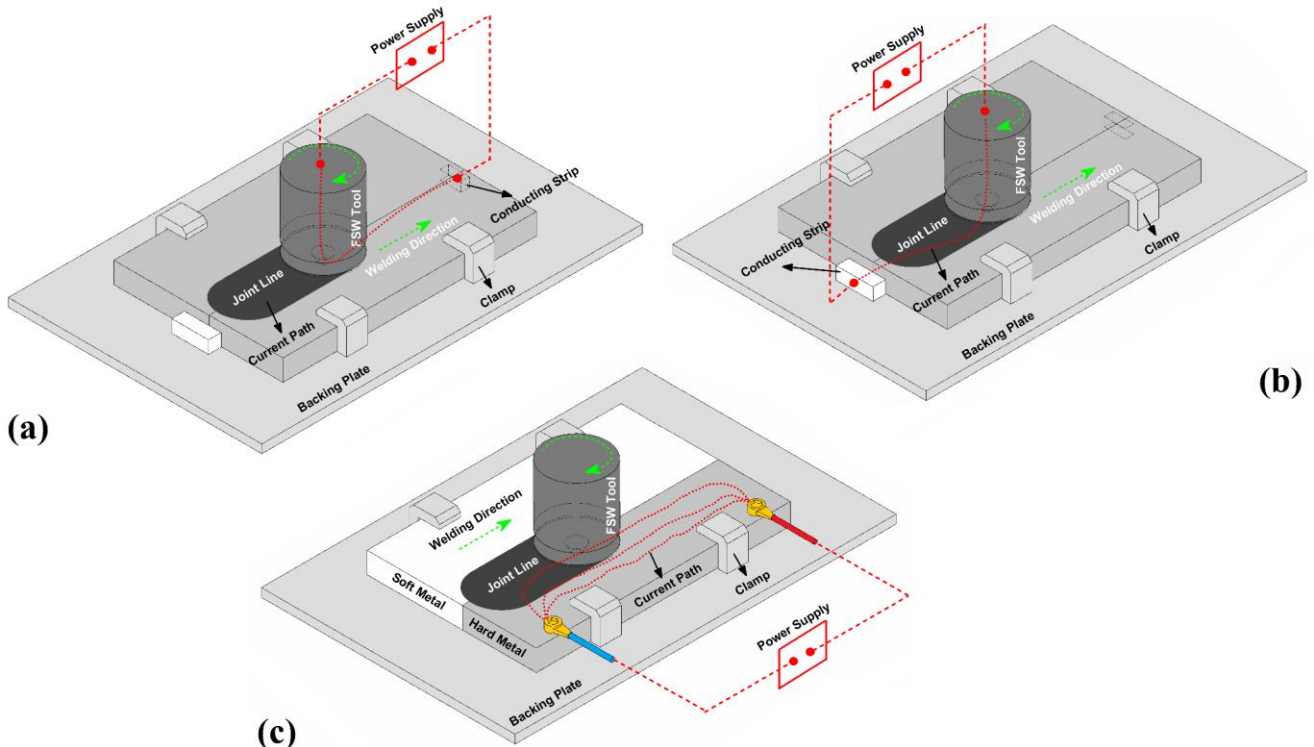


Figure 1. EA-FSW in (a) preheating, (b) heat treatment, and (c) combination models.

The classification in EA-FSW is related to the electrical current circuit. A power supply is used in the middle of the electrical line to create an electrical current flow into the joint line, on the side of the current attached to the FSW tool (usually positive side) and another side attached to a conductive strip. If the conductive strip is placed in front of the workpiece,

the electrical current is imported to the joint line by the tool and exits from the conductive strip in front of the tool. In this case, the electrical resistance heated the interfaces that were not welded, and electrical current could preheat the joint line before FSW (Figure 1a). In this type, the workpieces are preheated in front of the tool, which makes the joint line metal soft, and for this reason, this type is called preheating EA-FSW. For this reason, the welding force decreases sharply, the joining process time decreases, and the working life of the FSW tool is prolonged. The type one joint is suitable for hard materials that can be softened before the FSW tool mixes workpieces. In this case, the flowability during the stirring action increases with the decreasing shear strength of base metals. Greater flowability decreases the formation of root voids and prevents surface flash formation.

In the second type of EA-FSW, the conductive strip is placed behind the joint line (Figure 1b). In this case, the electrical current path is behind the FSW tool and causes the welded joint-line temperature to increase after welding, due to the inner resistance of the joint line. In this case, the conducting circuit caused a heat treatment effect on the joint line. In the second type of EA-FSW, the resistance heat produced by the electrical current reduces the residual stress of the joint line and the hardness, and improves the formability of the joint line for the post-metal-forming process. In this case, the joining mechanism is similar to the regular FSW, but with this type, a post-heat treatment is applied on the joint line and helps the microstructural recovery of weldments. The third type is related to the dissimilar joints (Figure 1c). In this case, the electrical current passes through harder materials to be heated up by resistance heat. In this process, the harder material became softer, and the welding procedure made a sound and defect-free joint line [24]. This type of joint increases the stirring of the hard material during dissimilar joining. The lack of mixing between dissimilar materials on the macroscale could be improved. On the other hand, overheating herded materials may lead to thick intermetallic compounds (IMC) forming, decreasing the final joint strength. Controlling input current to prevent the formation of thick IMC is the negative side of this joint.

4. Various Types of EA-FSW Tools

The tool used in the FSW process plays the leading role in joining metals. In the EA-FSW process, the tools are generally divided into four groups. The first group comprises simple tools, and electrical current flows on them from a conductive conductor. This type of tool is simple and similar to the conventional FSW process. A schematic view of a simple EA-FSW tool is depicted in Figure 2a (Type a). This type of tool was an early idea for joining by the EA-FSW process. Due to the electrical resistance of the tool material and heat transfer of the joint line by the tool, this type of tool is not very popular, because the temperature of the tool significantly increases, and it is hard to use this type of tool for a long time [24].

The second type is the tool with a conductive coil or core inside the tool. A conductive core (such as copper) in this tool type is placed inside the FSW tool. The thickness and conductivity of the materials inside the tool determine the electrical current flow and electrical heat input inside the joint line. A schematic view of the EA-FSW tool with a conductive core is depicted in Figure 2b (Type b). The third type of tool is developed from the first type of tool. In this type, the electrical current flows from the tool body, but the tool is not solid. A hole is contained inside the tool, and a coolant flows inside this hole. This mechanism is applied to decrease the tool temperature during the joining process. The coolant could be liquid (water or soap water) or gas (nitrogen or hydrogen) [23]. The flow of coolant decreased the tool temperature during the EA-FSW process. Figure 2c (Type c) presents the schematic view of the third tool type. The fourth type is the modern type of tools, which is presented in Figure 2d (Type d). In this category, tool type two or tool type three is equipped with an electromagnetic or ultrasound vibration system to decrease the limitations of various joining configurations or materials by EA-FSW. The material used as an EA-FSW tool is another parameter that can affect the joint's electrical current and final quality [25]. It is essential that the electrical current passes from the tool material, but

in the Type a tool, this has not had a significant effect on the final properties of the joint. The listed material used as an EA-FSW tool is presented in Table 1. A steel-based tool and tungsten-based tool are used during EA-FSW of similar joints. Table 1 presents the data ordering of the workpiece material.

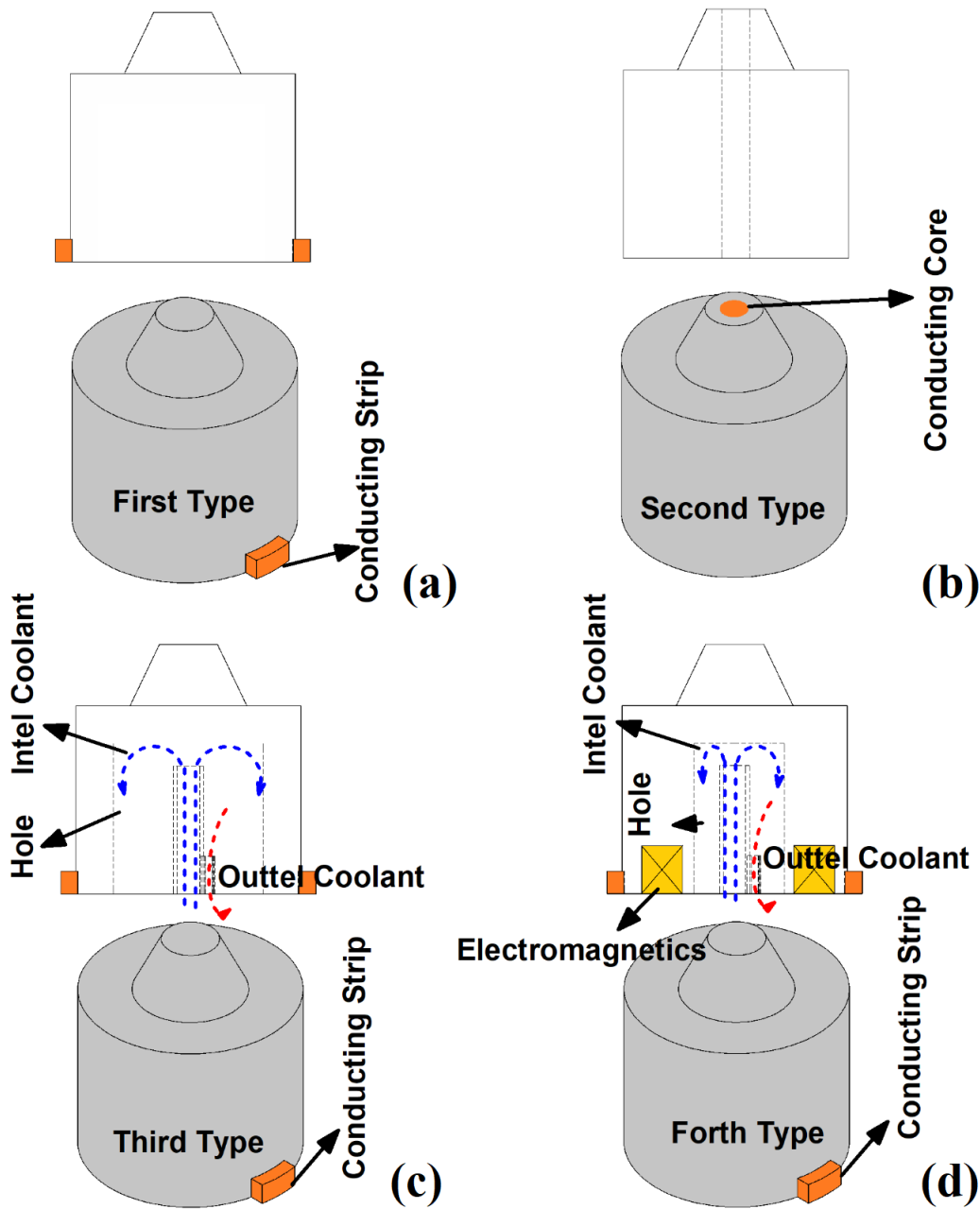


Figure 2. EA-FSW Tools, (a) Type a, (b) Type b, (c) Type c, and (d) Type d.

The first category is related to the EA-FSW joint of aluminum alloys and, after that, magnesium alloys and titanium alloys, and at the end, low-carbon steel and Inconel. In the available literature until this moment, limited research has been conducted on the EA-FSW process. From the process point of view, all tool types have been used in EA-FSW of similar joints, but when comparing them, tool Type a is the most popular. During EA-FSW, the rotational tool speed was kept constant, and just in low-carbon steel and Inconel joints, the rotational tool speed was selected as a variable. It seems the most critical factor during the EA-FSW process is the electrical current, for decreasing the strength of weldments, and the tool material should be conducive to desirable current resistance. The majority of

tools were tungsten-based and tool steel-based material. Tungsten-based tool materials were reported for welding titanium-based materials and Inconel materials. The maximum electrical current used during a similar EA-FSW joint was 720 A, and the lowest electrical current was reported to be 37.2 A. On the other hand, the most common current range was between 0 A and 150 A.

Table 1. Used tools and process parameters in EA-FSW of similar joints.

Tool Material	Type of Tool	Electrical Current	Rotational Velocity	Workpiece	Ref.
H-13 tool steel	Type a	Not mentioned	555 rpm	AA6061-T6511 aluminum	[26]
A2 tool steel	Type a	37.2 A	350 rpm	AA6061 aluminum	[27]
Not mentioned	Type c	720 A	1120 rpm	AA6082-T6 aluminum	[28]
H13 tool steel	Type b	720 A	1120 rpm	AA6082-T6 aluminum	[29]
Not mentioned	Type d	0–600 A	800 rpm	AA2219-T87 aluminum	[30]
T12 carbon tool steel	Type c	0–150 A	940 rpm	AA7075 aluminum	[31]
T12 carbon tool steel	Type c	0–150 A	1000 rpm	AZ31B Magnesium	[31]
H13 tool steel	Type a	0–400 A	800 rpm	AZ31B Magnesium	[32]
Not mentioned	Type a	0–200 A	1300 rpm	AZ31B Magnesium	[33]
Tungsten rhenium	Type d	100–300 A	200 rpm	Ti-6Al-4V Titanium	[34]
Tungsten rhenium	Type d	100–300 A	200 rpm	Ti-6Al-4V Titanium	[35]
Tungsten Carbide	Type a	50–150 A	500, 700 and 1000 rpm	Low carbon steel	[36–38]
Tungsten Carbide	Type a	50–150 A	600, 800 and 1000 rpm	Inconel 601	[39]

The situation in the dissimilar joint is different from similar joint cases. The various joints and related data collected from dissimilar EA-FSW joints are presented in Table 2. Due to limited data about EA-FSW joints between dissimilar materials, it can be seen that the rotational tool speed is much higher than the EA-FSW of similar joints. This is due to the second alloy's higher melting point and strength than the first one. The range of electrical current used is related to the base materials. The typical current used for a similar joint was below 720 A, while the electrical current used in a dissimilar joint reached 1000 A.

Table 2. Used tools and process parameters in EA-FSW of dissimilar joints.

Tool Material	Type of Tool	Electrical Current	Rotational Velocity	Workpiece	Ref.
Not mentioned	Type c	0–500 A	800–1500 rpm	AA6061 aluminum to AZ31B magnesium	[31]
T12 carbon tool steel	Type c	1000 A	1000 rpm	2Cr13Mn9Ni4 stainless steel to Q235B steel	[40]
XSYTIN-1	Type a	10 A	1800 rpm	AA6061-T6511 aluminum to 1018 mild steel	[41]
H13 tool steel	Type a	560 A	2000 rpm	AA6061-T6 aluminum to TRIP steel	[42]
H13 tool steel	Type a	Not mentioned	Not mentioned	7075-T6 aluminum to glass fiber-reinforced poly-ether-ether-ketone	[43]
Tungsten	Type a	400 mA	1200 rpm	high-density polyethylene (HDPE) to 316L stainless-steel textile	[44]

On the other hand, the tools with Type a and Type c were used in dissimilar joints. The current and tool rotational velocity can determine the soundness of final joints. The typical tool material used for dissimilar EA-FSW was tool steel. The ceramic composite material introduced as the XSYTIN-1 alloy was the specific material used for an EA-FSW

tool when joining aluminum to steel. By comparing the data, any relation between tool material and used electrical current or rotational velocity cannot be found. The collected data indicate that the lowest electrical current (37.2 A) was used with the A2 tool steel during the joining of AA6061 aluminum alloy, and the highest electrical current (1000 A) was used for dissimilar EA-FSW during the joining of 2Cr13Mn9Ni4 stainless steel to Q235B steel. The harder materials need a higher electrical current to become soft, and softer materials need a lower electrical current.

During EA-FSW, the researchers selected the joint type of the tool type related to the final properties of the joint. By selecting various joint types, the joint line can be affected by electrical current. During the welding procedure, the joint line can be affected by external heat. Selecting various tools during the joining procedure leads to local change by the electrical current. The electrical current is inserted into the stir zone when the tool type procedure is selected, and in this case, the additional heat can change the stirring phenomena inside the stir zone. Two points in the tool type process are not detailed, and they are what would be the best procedure for selecting the tool's material and calculating the electrical current range. The materials of the tool can affect the heat transfer phenomena at the stir zone during joining, and an electrical current can show how much additional heat is inserted into the joint line. Due to the lack of research reports on thermal history during EA-FSW, these questions are unknown.

5. EA-FSW of Similar Joints

A similar joint refers to a joint with the same base materials welded together. In such a case, the EA-FSW can be divided into two groups [45]. The electrical current was applied to the base materials and on the joint line throughout the tool. The collection data about various joint types in EA-FSW of similar joints are presented in Table 3. The Inconel 601 was the thinnest plate (2 mm) welded by EA-FSW, and the AA2219-T87 aluminum alloy was the thickest plate (6 mm). Most joints currently use electrical tools to add extra heat to the joint line; in other cases, the preheating EA-FSW case was mostly used. On the other hand, the output results of EA-FSW joints were mostly focused on material flow and hardness of the joint.

Table 3. Used joint types during EA-FSW of similar joints.

Raw Material	Thickness	Type of Joint	Output Results	Ref.
AA6061-T6511 aluminum	0.25 in	Combination	Force, temperature, and hardness	[26]
AA6061 aluminum	3.175 mm	Combination	Force and torque	[27]
AA6082-T6 aluminum	4 mm	Simple	Heat and material flow	[28]
AA6082-T6 aluminum	4 mm	Simple	Heat and material flow	[29]
AA2219-T87 aluminum	6 mm	Simple	Material flow and mechanical properties	[30]
AA7075 aluminum	5 mm	Preheat	Microstructure and hardness analysis	[31]
AZ31B magnesium	5 mm	Preheat	Microstructure and hardness analysis	[31]
AZ31B magnesium	3 mm	Preheat	Material flow and mechanical properties	[32]
AZ31B magnesium	5 mm	Simple	Material flow and mechanical properties	[33]
Ti-6Al-4V titanium	3 mm	Simple	Material flow and mechanical properties	[34]
Ti-6Al-4V titanium	3 mm	Simple	Microstructure analysis	[35]
Low-carbon steel	Not mentioned	Preheat	Hardness analysis	[36–38]
Inconel 601	2 mm	Simple	Tensile strength	[39]

5.1. EA-FSW of Aluminium Alloys

Aluminum alloys are widely used in various industries due to their lower melting temperature compared with other metals, outstanding mechanical performance, good weldability, and high corrosion resistance [46]. Until now, two pieces of literature considered EA-FSW of aluminum alloys. The lack of penetration (LOP) defects in the conventional FSW process appear at the bottom of the stir zone [47]. LOP is a common defect in the FSW of aluminum alloys that formed due to a slightly shorter pin length than the thickness of the weld metals. The LOP results from poor material flow at the bottom of base materials. The study on the effects of electrical current assistance on the LOP during the FSW of aluminum alloy was considered for the first time by Chen et al. [28]. They performed 800A electrical current during FSW of the AA6082-T6 aluminum alloy sheet. The result shows that the electrical current during FSW effectively reduced the LOP defect at the root of the stir zone. The higher heat input in the stir zone caused the materials to flow and increase in the root of the stir zone. The electrical resistance of the joint line increased the internal heat, and the aluminum alloy was plasticized further. The higher plasticized phase means the softening and stirring actions to soften the metals are easier.

Santos et al. [29] investigated the EA-FSW of 4 mm-thick AA6082-T6 aluminum alloy. Root defects are common when aluminum alloys are welded using a friction stir welding process. The lack of penetration and the alignment of oxide particles and/or second-phase particles are common root defects in this case, where the latter is more difficult to detect and eliminate. Machining the root and double-sided welding using bobbin tool welding are examples presented in the literature to overcome these defects. The application of a high-density electrical current in FSW promotes viscoplasticity of the material, and the probability of the formation of root defects decreases as a result. Chen et al. [30] investigated various input electric currents on the properties of the AA2219 aluminum alloy EA-FSW joint. They tested the 0–600 A direct current on the mechanical properties of the final joint. The first difference between the joint welded by FSW and EA-FSW was that the temperature difference in the advancing side (AS) and retreating side (RS) in EA-FSW was more than in the FSW case. The hardness of the joint welded by EA-FSW was also greater than the FSW case. In the electrical current range used by Chen et al., the joint welded with 100–400 A has improved tensile strength by 2.74–7.38%, respectively, but the joint welded by 600A has significantly improved tensile strength by 17.11%. They also reported that it promoted hardness for weld zones, especially on the advancing side. Higher joint strength was achieved when higher current intensity was applied (500 A to 600 A). The bigger overall joint area and especially bigger thermo-mechanical affected zone (TMAZ) and heat affected zone (HAZ) and weld nugget zone (WNZ) were evident in the joints. The failure zone was the boundary of the nugget zone and TMAZ on the advancing side, and the nugget zone on the retreading side for FSW- and EA-FSW-welded joints, respectively. The discontinuity of different zones in the microstructure is the reason of starting failure in this zone. When a higher current intensity is used, the dimples are larger and deeper. Larger and deeper dimples are formed when the material represents more ductile behavior under loading. When a higher current is applied, the material is deformed in a higher temperature which maintains its ductility. A refinement of Al_2Cu precipitates and more homogenous distribution of them are results of applying an electrical current. When an electrical current is introduced to the nugget, the material experiences a higher temperature, which makes it less strong, and with the application of a lower shear stress it is possible to flow the material. This results in more homogenous distribution of reinforcing particles. The cross-section view of EA-FSWed joints by Chen et al. [30] is presented in Figure 3. Applying electrical current also is beneficial in many aspects; however, due to increased heat input, grain growth is evident. For example, Luo et al. [31] investigated EA-FSW of Al 7075 butt welds with a thickness of 5 mm. They reported an increase in the grain size from 7–11 μm , increasing the current intensity. In HAZ, grain coarsening was observed by applying the current intensity. In the case of EA-FSW, proper welding

parameters such as tool rotational speed and tool travel speed should be considered to prevent overheating of the joint.

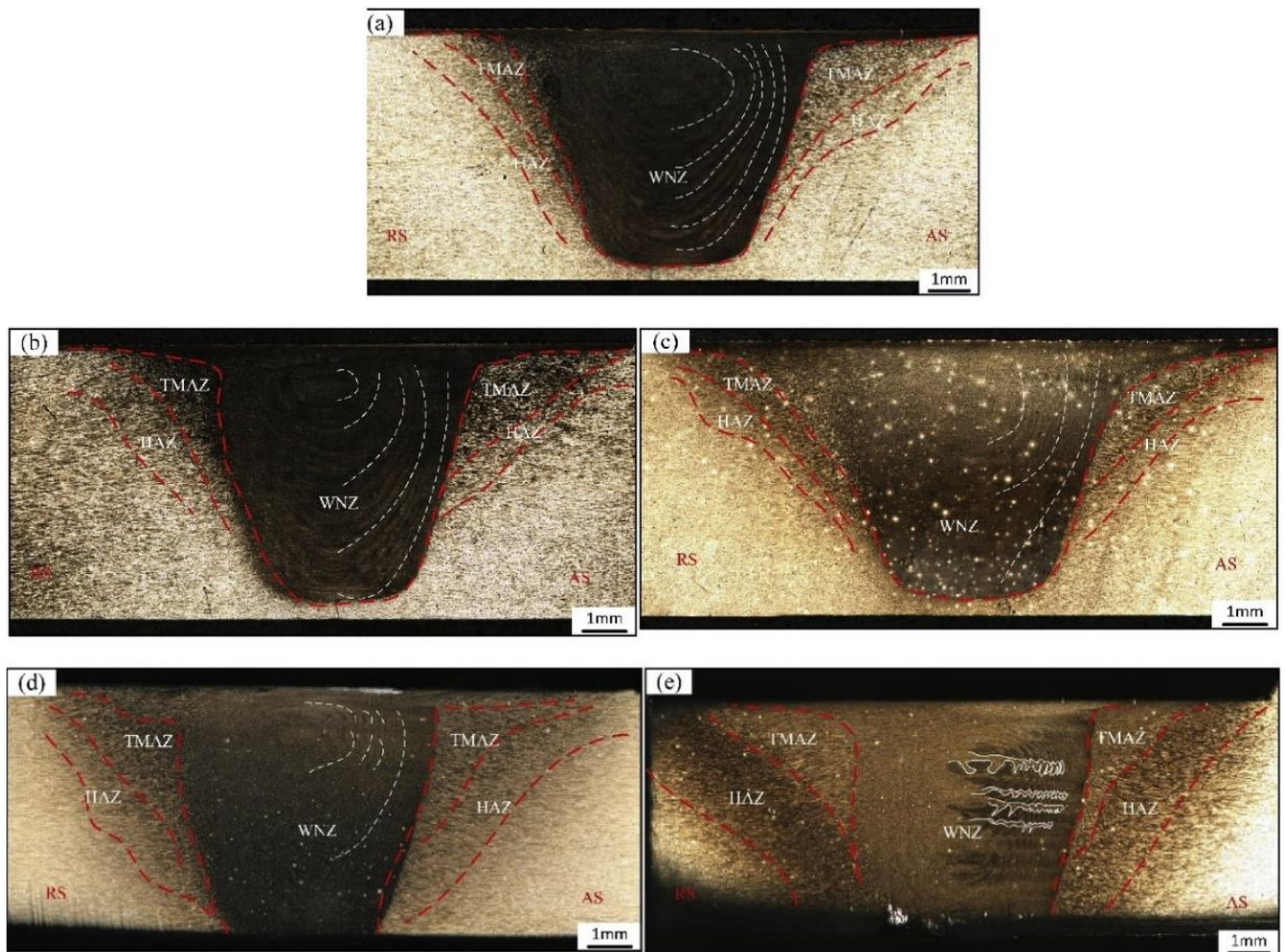


Figure 3. Macroscopic morphology of EA-FSWed joints of AA2219 using a current of (a) 0 A, (b) 200 A, (c) 400 A, (d) 500 A, (e) 600 A. The white dotted lines present the material flow direction. Reprinted with permission from ref. [30]. Copyright 2022 Elsevier.

5.2. EA-FSW of Magnesium Alloys

Some of the outstanding properties of magnesium alloys, that make them an interesting grade of alloys to be used in various industrial sectors and especially the transportation sector, are high strength-to-mass ratio, good heat dissipation performance, and good shock absorption performance. Luo et al. [31] investigated EA-FSW of AZ31B butt welds with a thickness of 5 mm. they reported nano-size grains in the stir zone when the current intensity was less than 150 A. They also reported the presence of twin crystals and a more uniform microstructure in TMAZ in this range. However, the coarsening of the microstructure was reported in the HAZ.

Han et al. [33] investigated the EA-FSW of the AZ31B magnesium alloy. They reported a larger welding zone and a more homogenous microstructure with a higher joint strength due to applying an electric current of up to 200 A. They used 0 A, 100 A, and 200 A electrical currents and demonstrated that all joints were formed without defects and voids. With an increasing electrical current, the heat input on the joint line increased, and bigger HAZ and stir zone (SZ) were formed in the 200 A case compared with other samples. The joint grain size decreases with increasing electrical current. The smaller grain size increased the joint

hardness and mechanical properties of the AZ31B magnesium alloy joint. The FSW joint fractured from the HAZ area, while the EA-FSW cases fractured from the SZ area after the tensile test.

Chen et al. [32] investigated welding of the same alloy but using a pulse current, and reported similar results. In the experiments, they increased the electrical current to 400 A during EA-FSW of the AZ31B magnesium alloy. The SZ and HAZ thickness increased by increasing electrical current, and the biggest joint was formed in the 400 A case. They show that the intermetallic compounds (IMC) were formed with increasing electrical current in SZ. Increasing the temperature promotes the formation of IMCs. When an electric current is used, the temperature in the nugget increases, which leads to the formation of IMCs, or makes them thicker. According to X-ray powder diffraction (XRD) results, Mg and $\text{Al}_{12}\text{Mg}_{17}$ were formed in a joint line. The IMC formation in this sample is related to the preheating joint that Chen et al. [32] used. They used the preheating EA-FSW joint, while Han et al. [33] used tool Type c to conduct EA-FSW. Due to this difference, the fracture location of welded samples in Chen et al.'s [32] tests differed. In this case, the fracture location of the AZ31B magnesium alloy was the HAZ area.

5.3. EA-FSW of Titanium Alloys

Friction stir welding is a promising welding procedure when joining light metals, especially aluminum alloys. However, when high-melting-point metals such as steel and titanium are to be welded, in many cases, there is not enough heat input during the welding procedure. Thus, applying auxiliary heat sources such as high-density current helps achieve the targeted temperature and plasticity. Han et al. [34] investigated the electrically assisted friction stir welding of Ti6Al4V joints. They indicated that the tensile properties of the joint improved when using electrically assisted friction stir welding, with no loss of ductility due to homogeneity of the microstructure and strain, dissolution of the beta phase, and random orientations. They reported that some slip systems are activated just when an electrical current is applied, which is attributed to the higher temperature and deformation strain as a result of the thermal effect of the electrical current. They suggested the application of 200 A as the optimum current density.

The same titanium alloy was also investigated by Jiang et al. [35]. They also reported a smooth change in the microstructure of the joints when electrically current assisted friction stir welding is applied, and random distribution in the stir zone. Improvement in the tensile properties of the joint was also indicated. They reported slightly larger grains in the advanced side of the stir zone compared with the retreating side, which was illustrated by some other authors in welding other alloys, too. They also reported a slightly more robust dynamic recovery in the HAZ, and dynamic recrystallization in the SZ for FSW in comparison with EA-FSW. They suggested the increasing loss rate of elemental Al and larger grains as a reason for the decrease in the hardness. They reported better fatigue performance for the electrically assisted joints with a current intensity of 100 A due to smaller macro zones than conventional friction stir welding. Any increase in the current intensity results in a more homogenous distribution of hardness.

5.4. EA-FSW of Steels

Steels have been widely used in many industries for a long time. The effect of electrical-assisted FSW can give a new opportunity for producing a more substantial structure. The available information about the EA-FSW of steels is limited. Chowdhury et al. [36] used AC and DC to weld carbon steel plates with a preheating approach. They used the 50–150 A current range with 500–1000 rpm and reported the ultimate tensile strength of the joint. Based on their results, the EA-FSW can improve the mechanical properties of joints. Moreover, the DC effect on the tensile strength of the joint is greater than the AC. They started with 100 rpm tool rotation and 50 A current (DC), and the joint efficacy reached 109% [37].

5.5. EA-FSW of Inconel

The only research output about the EA-FSW of Inconel is related to the study by Sengupta et al. [39]. The investigated wear of the tungsten carbide (WC) tool during EA-FSW of Inconel 601. The electrical current range was 50–150 A, and the tool rotational velocity was 900–1100 rpm, and the process was performed by a preheating approach. In the first stage, they reported that with 150 A and 1100 rpm, the joint efficacy of Inconel 601 reaches 105%, which is a huge increase, and means the joint strength after EA-FSW increases more than the base metal. Due to the high temperature and corrosion resistance of Inconel 601, the tool wear can waste money and process time during FSW. Sengupta et al. [39] collected the WC tool's wear rates concerning tool rotational and traversed velocity and compared them in the case of FSW with EA-FSW. Figure 4 shows their results on the wear rate of the FSW tool in the FSW and EA-FSW cases. They did not report the depth analysis of their results and stated that electrical assistance improves the wear properties of the WC tool. In Figure 4, the Y-axis on the left shows the FSW tool rotational speed (rpm), and the right shows tool wear (mg/m).

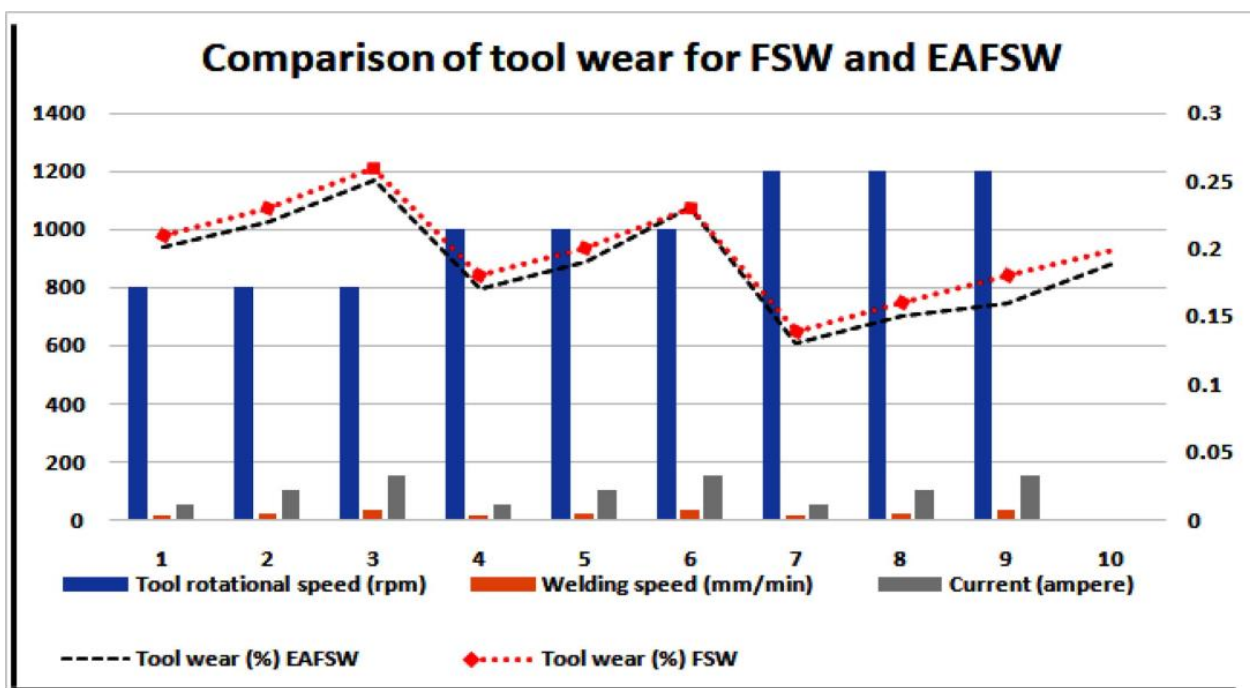


Figure 4. Comparison of wear of WC tool in FSW and EA-FSW samples. Reprinted with permission from ref. [39]. Copyright 2022 Elsevier.

6. EA-FSW of Dissimilar Joints

Solid-state welding procedures, especially friction stir welding, are a great choice when joining dissimilar or metallic alloys to join polymers [24]. In this case, an external heat source such as an electrical current could be pretty beneficial to minimize or eliminate joint defects. These defects are prevalent, especially in the root zone when joining is carried out in lap configuration. On the other hand, the chemical bonding at the interface of base materials could change the presence of electrical current. Several authors investigated dissimilar joining procedures using FSW, and the reported literature is minimal in the case of EA-FSW. Table 4 lists the dissimilar joints prepared by the EA-FSW process. The case studies joined by EA-FSW included aluminum–magnesium, steel–steel, aluminum–steel, polymer–aluminum, and polymer–steel. The preheat and combination type process was used in this category, and the thicknesses of raw sheets were 2 mm and 3 mm.

Table 4. Dissimilar joints welded by EA-FSW.

Raw Material	Thickness	Type of Joint	Output Results	Ref.
AA6061 aluminum to AZ31B magnesium	3 mm	Preheat	Material flow and mechanical properties	[31]
2Cr13Mn9Ni4 stainless steel to Q235B steel	2 mm	Preheat	Microstructure	[40]
AA6061-T6511 aluminum to 1018 mild steel	3 mm	Combine	Material flow and mechanical properties	[41]
AA6061-T6 aluminum to TRIP steel	2 mm	Combine	Material flow and mechanical properties	[42]
7075-T6 aluminum to glass fiber-reinforced poly-ether-ether-ketone	2 mm	Combine	Material flow and mechanical properties	[43]
high-density polyethylene (HDPE) to 316L stainless-steel textile	3 mm	Combine	Material flow and mechanical properties	[44]

6.1. EA-FSW of Dissimilar Steels

Luo et al. [31] investigated EA-FSW of 2 mm-thick plates of 2Cr13Mn9Ni4 stainless steel and Q235B steel in lap configuration. Tool rotational speed of 1000 rpm, tool traverse speed of 50 mm/min, and current intensity of 1000 A were the welding parameters used in this case. They indicated that it is feasible to join high-strength alloys without tool damage. Due to the high shear strength of steels, the wear rate in the FSW process is high. Luo et al. [31] showed that EA-FSW could minimize tool damage during welding. They stated that no gap or voids formed at the EA-FSW joint interface, and the mechanical interlock's hardness was higher than the base metals. The mechanical interlock in the 2Cr13Mn9Ni4 stainless steel and Q235B steel joint welded by EA-FSW was greater than the FSW case.

Sengupta et al. [38] studied the EA-FSW of IS 2062 Grade B and 316 stainless steel. The aim of their research was the optimization of process parameters in order to obtain the maximum possible tensile strength and lowest tool wear. They used the same process parameters for FSW and EA-FSW to compare the effects of electric current. The rotational tool speed, traveling velocity, and electrical current were 500–1050 rpm, 11–24 mm/min, and 50–150 A, respectively. This research was based on statistics, and they did not report deep analysis or characterization of their welded samples. The maximum tensile strength was achieved at 650 rpm, 20 mm/min, and 150 A has 452 MPa. The lowest tool wear was recorded in the same process parameter by 0.07%, while the wear of the tool in the FSW sample with the same process parameter was 0.11%.

6.2. EA-FSW of Aluminum to Steel

Aluminum–steel joints are the most popular joint produced by the FSW process. Due to the combination of base metals properties, the produced structure can be solid and lightweight. For this reason, the EA-FSW can improve the quality of this joint to reach a higher strength. Liu et al. [48] investigated a dissimilar joint between AA16061 aluminum alloy and TRIP 780 steel by EA-FSW. They introduced a method where there is no need for the tool to be used as one of the electrodes, when in many similar procedures it is. They reported a significant reduction in the axial load applying the high-density current. They also reported the presence of micro interlocking in the joint's microstructure, which is considered beneficial for the joint quality. They concluded a promotion by forming a thin layer of IMC for the plunge section of the joint. The reason is the combined effect of accelerated atom diffusion and reduced activation energy for chemical reactions. The thickness of IMC in the EA-FSW case was similar to the FSW process with a high tool rotational speed. The electrical current helps decrease the shear strength of the base metal and increase the aluminum and steel interaction at the joint interface. The comparison between the IMC thickness of FSW and EA-FSW at the interface of the AA16061 aluminum alloy to TRIP 780 steel is presented in Figure 5.

Chen et al. [42] investigated the electrical current effects on the quality of dissimilar joints between aluminum alloy and advanced high-strength steel utilizing friction stir spot welding. In their setup, the aluminum alloy was placed on top, and the steel was

placed at the bottom. They tried two approaches. First, they put two electrodes for passing electrical current on the top plate. In the second approach, they put one electrode on the top plate and the second on the bottom plate. They reported that using electrical current decreases the plunging force during the joining process and improves the joint strength. The average force value during electrical-assisted welding was near 13% less than without an electrical-assisted case. The electrical assist increased the aluminum flow in SZ, and the diffusion of aluminum elements in IMC increased.

Shaffer et al. [41] used two different tool materials and evaluated their effects on EA-FSW of the AA6061 aluminum alloy to mild steel. They made the FSW tool from tool steel and XSYTIN-1 ceramic base material. They stated that ceramic material decreases the maximum temperature in joint lines and the joint strength decreases. This change was related to the change in friction coefficient at the interface of the tool and workpieces. A lower friction coefficient at the interface of the XSYTIN-1 ceramic material with aluminum and steel leads to lower heat generation.

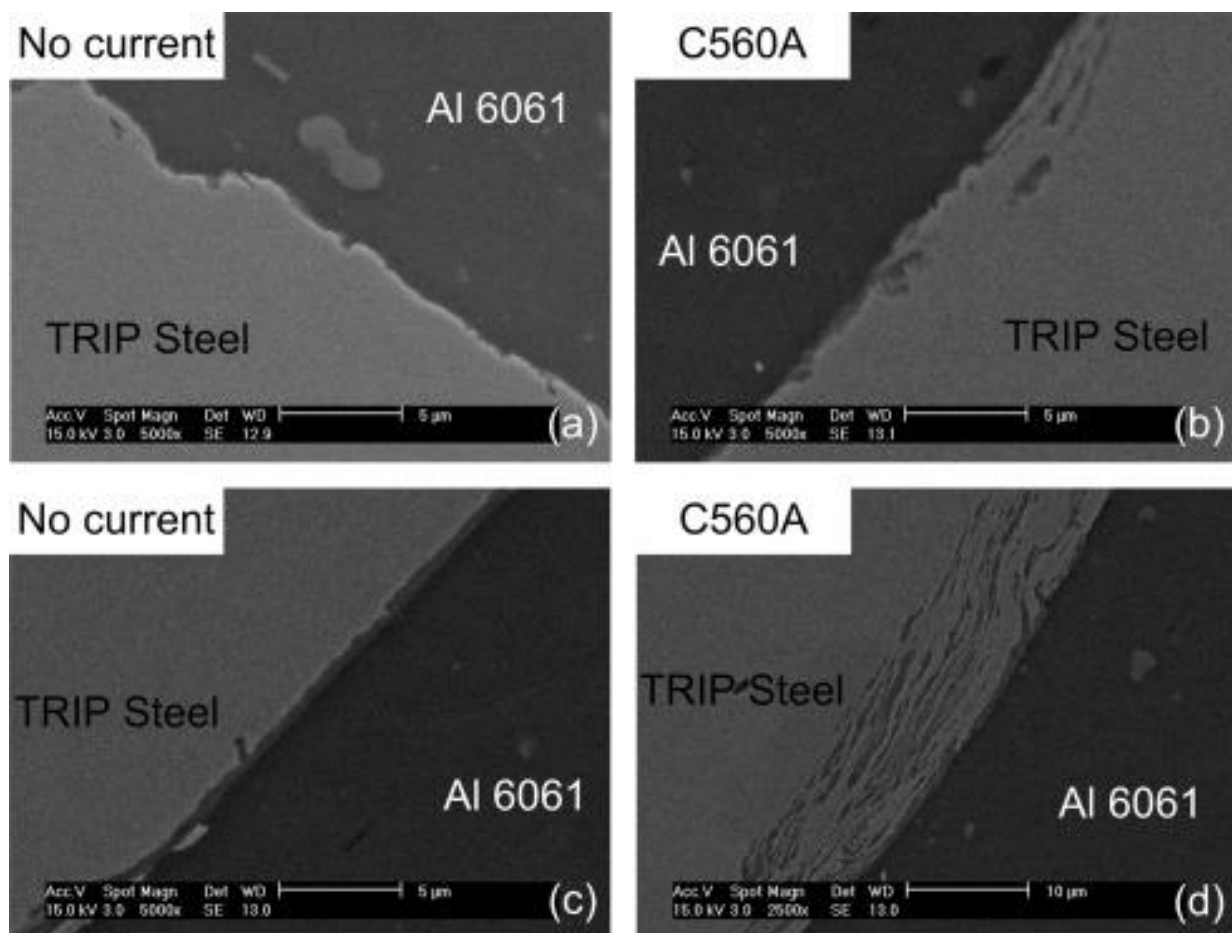


Figure 5. IMC thickness at interface of aluminum alloy and steel in (a) upper area and (b) lower area of FSW joint. Reprinted with permission from ref. [48]. Copyright 2022 Elsevier. IMC thickness at interface of aluminum alloy and steel in (c) upper area and (d) lower area of EA-FSW joint. Reprinted with permission from ref. [48]. Copyright 2022 Elsevier.

6.3. EA-FSW of Polymer to Steel

Metal polymer joints are considered an exciting topic in automobile industries. The joining between polymeric materials and metals gives an outstanding opportunity to produce a lightweight structure with a big concern about fuel consumption. A considerable difference between melting point and physical properties leads to immiscibility. In such cases, joining polymeric materials and metallics materials is very hard. Even using the FSW

process, joining these materials is challenging and complicated. The FSW process is one of the last solutions for joining these materials.

For this reason, EA-FSW would be a new approach to increase the joint strength and quality of metal–polymer joints. As an early step, Aghajani Derazkola et al. [44] tried to join stainless-steel textiles with high-density polyethylene (HDPE). They used 400 mA electrical current on the steel side, then joined the HDPE and steel. They show that the electrical current helps the chemical bond between steel and HDPE. The electrical current decreases the shear strength of stainless steel and helps improve material flow in the joint area. One of the new achievements in this research was changing the electrical current during the joining process. In this research, they used a combination joint type, showing that, with the forward moving of the tool, the steel textile was torn by the tool, and steel particles spread on the polymer matrix. This phenomenon changes the electrical heat in a different joint line area. In this case, the steel textile area that can pass the electrical current decreases. The description of steel textile consumption and its effect on the thermal history of the different parts of the joint is shown in Figure 6. They used three thermocouples on the joint line. The result shows that the maximum temperature at the front of the tool decreases slightly by passing the tool before the tool reaches thermocouple 1 (N1), and the recorded heat reaches maximum. After passing from the N1 position, the steel textile is consumed, and the area that passes the electrical current decreases. With this decrease, the heat generation by electrical resistance decreases. This trend is also repeated in the thermocouple 2 (N2) and thermocouple 3 (N3) results. It was the first time that the electrical current was changed by consuming raw material. The details for changing the recorded heat during the procedure are depicted in Figure 6c. At first, the tool starts moving forward, and the amount of stainless steel is torn and extruded into the stir zone. In this case, the torn stainless-steel textile area (MSST) cannot transfer electricity and the total heat produced by passing electrical current with residual stainless-steel textile (RSST). These changes, while the tool moves forward, decrease the total amount of heat in N1, N2, and N3 thermocouples.

6.4. EA-FSW of Aluminum to Magnesium

The aluminum–magnesium joint is also an exciting joint recently considered a reinforced structure in aero structure, automobile, and railway components. The research on FSW of aluminum alloys and magnesium alloys has recently increased. Combining these two alloys leads to the formation of a strong structure. The only research on EA-FSW of aluminum alloy and magnesium was carried out by Xiaoqing et al. [40]. They used different electric currents, tool rotational velocities, and traverse velocities of the tool. They indicated that electrical current assistance helps raw materials' fluid-ability and removes the possible defects that may form in the FSW sample. In this case, they stated that the root void forms in the FSW joint, and this root is removed with the increased electrical current. With the increasing electrical current of more than 300 A, minor defects form at the interface of the stir zone and aluminum alloy. Figure 7 presented the cross-section view of samples that welded 0 A, 300 A, and 500 A. The dashed circles show the formed voids in the stir zone. As can be seen, a significant void formed at the root of the joint with 0A electrical current. The size of voids decreased in the 300 A electrical current joint, but they formed in the root of the stir zone. When increasing the electrical current to 500 A, the voids' size significantly decreases and forms at the interface aluminum alloy and stir zone. On the other hand, the formation of IMC at the interface of the base metal would harm the mechanical properties. They stated that in the FSW case, various particles and bands are formed, and when applying the electrical current, the IMC thickness decreased. The IMC in the FSW case had a cloud shape, and in the 300 A EA-FSW case, the IMC shape at the interface of base metals changed to a stream shape. In the 500 A EA-FSW case, the IMC numbers decreased, and sandwich structures formed at the interface. The sandwich structure comprised thin Al-IMC-Mg structures.

6.5. EA-FSW of Aluminum to Polymer

Li et al. [43] investigated the application of electrical current in welding a hybrid 7075 aluminum alloy-SGF/PEEK polymer matrix joint. They proposed a new variant of solid-state welding called top-thermic friction stir lap welding (TT-FSLP). In this process, two strips are used on top of the upper plate to provide resistance heating. The process eliminates defects that are present in the conventional process. In the conventional lap welding, some defects are detectable, and, even though the process takes place with no defects during the joining process, after welding, due to the relaxation of residual stresses, some defects are present that drop the joint strength significantly. In TT-FSLP, two heating strips are placed on top of the upper plate, making it possible to use lower tool rotational speed with no drop in the heat input and produce a joint with no defects.

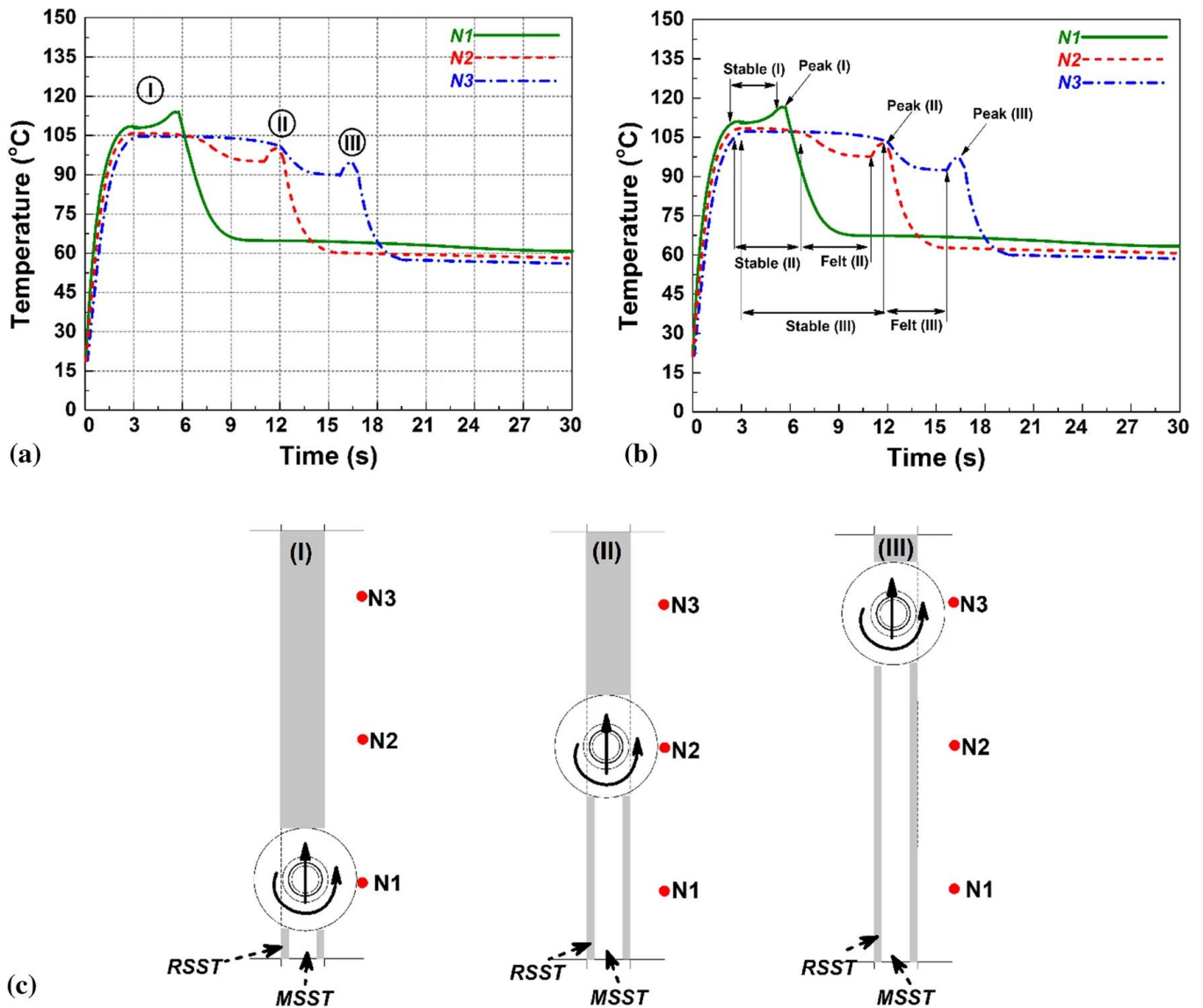


Figure 6. (a) Recorded temperature by different thermocouples, (b) different phase of thermal history, (c) schematic view of different phase of FSJ tool in phase (I), (II), and (III) Reprinted with permission from ref. [44]. Copyright 2022 Springer Nature.

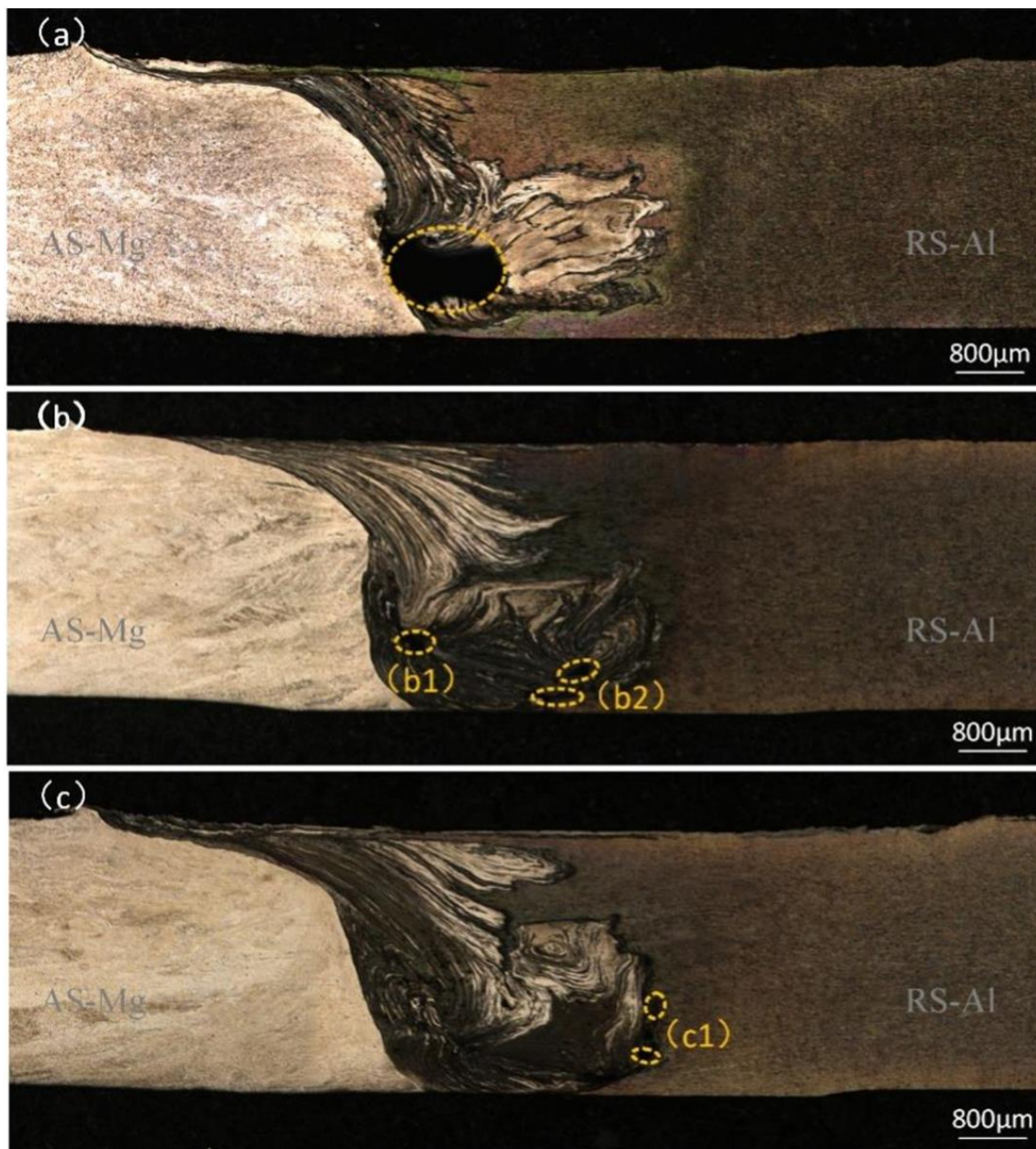


Figure 7. Cross-section view of Al-Mg joint welded by (a) 0 A, (b) 300 A, and (c) 500 A electrical current. Reprinted with permission from ref. [40]. Copyright 2022 Elsevier.

7. Simulation and Modelling of EA-FSW

Modeling is essential when a manufacturing process is to be investigated [49]. In these processes, generally, many parameters should be considered and evaluated. Analytical models are beneficial; however, due to the complexity of manufacturing processes, the numerical model could be more precise [50]. Friction stir welding and resistance welding, as two popular welding procedures, are investigated widely. However, electrically assisted friction stir welding could be considered a hybrid process where resistance welding and friction stir welding are jointly applied, because it is a new procedure, and very few investigations have been carried out.

Santos et al. [28] developed an analytical model together with a numerical one to investigate electrically assisted friction stir welding of the AA6082-T6 alloy. In their analytical model, the temperature rise due to the Joule effect is calculated considering the two following assumptions:

1. The electric current I (A) flows within the copper core of the probe, as depicted in Figure 6, with a diameter ϕ (m) at a distance h (m) from the back plate, closing the electric circuit;
2. The increase in the temperature that occurs due to the Joule effect under adiabatic conditions, that is, energy losses to adjacent materials (back plate, base materials, and tool) is negligible.

Thus, in the control volume, the temperature is raised using all heat generated by the Joule effect according to the fundamental calorimetric equation (Equation (2)):

$$Q_{\text{Joule effect}} = Q_{\text{Increase temperature}} \quad (1)$$

$$R \cdot I^2 \cdot t = m \cdot C_p \cdot \Delta T \quad (2)$$

where R [Ω] is the material electrical resistance, I [A] is the current intensity, t [s] is the time for passing the current, m [kg] is the mass dissipating heat, C_p [J/kg $^\circ$ C] is the specific heat of the material, and ΔT [$^\circ$ C] is the increment in temperature. Equation (3) could be used to calculate the electrical resistance:

$$R = \frac{h \cdot \rho_e}{\pi \phi^2 / 4} \quad (3)$$

where h [m] is the inherent gap distance, ρ_e [Ω m] is the electrical resistivity, and ϕ [m] is the diameter of the conducting copper core. The interaction time t [s] is related to the welding speed (V_x) [m/s] and can be calculated by Equation (4), considering that there is no complete overlapping between the copper core and the material interaction area during time t . The mass m [kg] is given by Equation (5), considering the geometrical features of the copper core (ϕ), gap distance (h), and the material density ρ [kg/m 3]:

$$t = \frac{\phi}{V_x} \quad (4)$$

$$m = \rho \cdot h \cdot \frac{\pi \phi^2}{4} \quad (5)$$

Thus, the temperature increase considering the Joule effect could be written as follows:

$$\Delta T = \frac{16}{\pi^2} \cdot \frac{\rho_e}{\rho \cdot C_p} \cdot \frac{1}{V_x} \cdot \frac{1}{\phi^3} \cdot I^2 \quad (6)$$

where the four affecting properties are as follows: $\frac{\rho_e}{\rho \cdot C_p}$ is the material properties, FSW travel speed V_x , geometric features of copper core diameter ϕ^3 , and electrical current intensity I^2 .

This heat source (Joule effect) is the third source in addition to the friction and plastic deformation that exists in the conventional FSW. Thus, a smaller probe diameter and higher current intensity results in a higher temperature raise in the nugget. The temperature raise, in practice, is higher compared with the values predicted by the model due to the decrease in the electrical conductivity of copper by the temperature raise. Santos et al. [28] also simulated the process using the CST-EM Studio Suit software. They included that the current intensity flows the layer below the probe tip by 70%. The simulation procedure and results are presented in Figure 8.

Long and Khanna [51] investigated EA-FSW numerically using finite element analysis. They reported reduced axial force in the penetration stage when an electrical current is applied, which may result in the promotion of tool wearing and a possibility to perform the welding with a speed that is twice that in conventional friction stir welding. Liu et al. [48] also simulated current density distribution and associated resistance heating using COMSOL Multiphysics software. The basic finite element code used by them is the code that was used to simulate resistance spot welding. The code was modified to analyze the process in two stages: penetration and welding. They presented governing equations as follows.

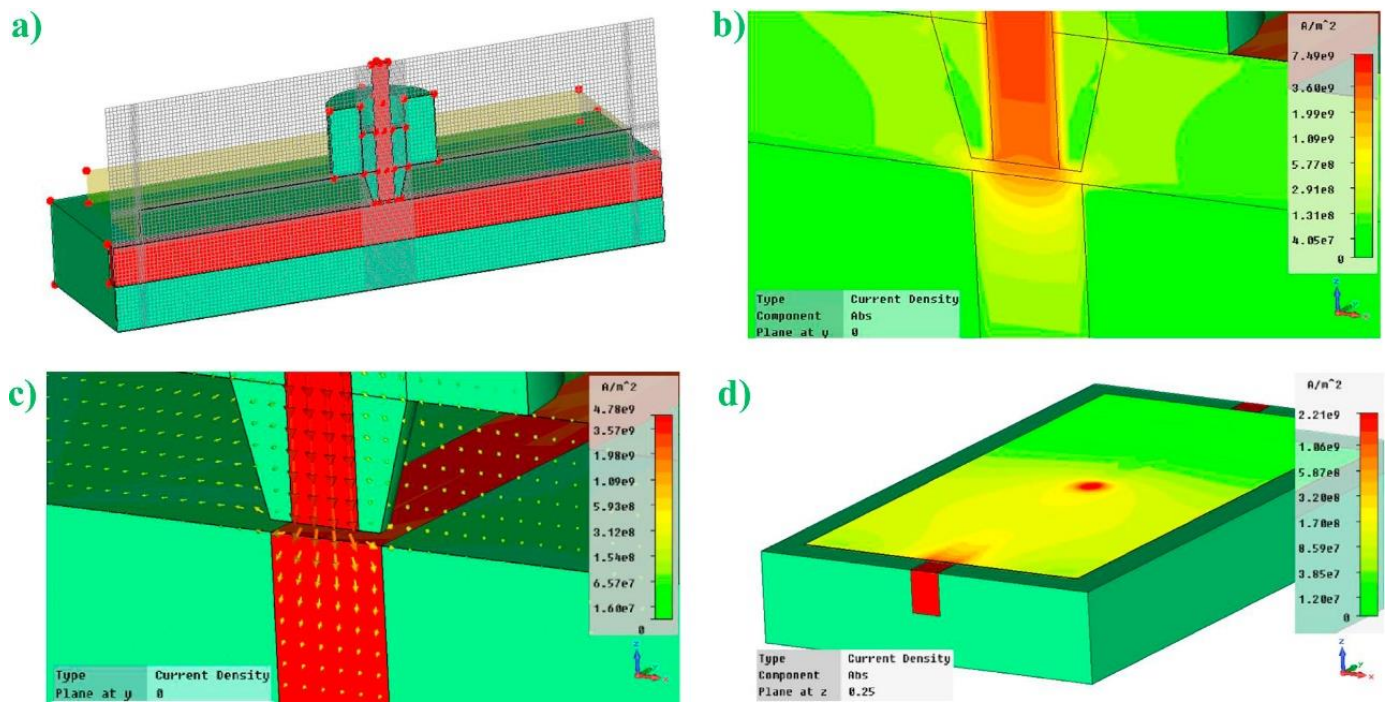


Figure 8. Numerical simulation of the current density distribution. (a) Geometrical model and mesh, (b) transversal cut view, (c) vectorial representation of the previous, and (d) top view. Reprinted with permission from ref. [29]. Copyright 2022 Elsevier.

Analyzing this process includes electrical, thermal, and mechanical problems. The Fourier’s 2nd law of heat transfer was used to model the heat transfer as follows:

$$\rho c \frac{\partial T}{\partial t} = k \left(\frac{\partial^2 T}{\partial x^2} + \frac{\partial^2 T}{\partial y^2} + \frac{\partial^2 T}{\partial z^2} \right) + q_0 \tag{7}$$

where ρ is the material density, c is the heat capacity, T is temperature, t is time, k is thermal conductivity, and q_0 is the inner heat source. c is a temperature-dependent material property. In this model, heat transfer attributed to the material motion is not considered. q_0 includes three kinds of heat sources as follows:

$$q_0 = q_{0F} + q_{0P} + q_{0R} \tag{8}$$

where q_{0F} is the friction heat, q_{0P} is plastic work heat, and q_{0R} is electrical resistance heat. There are two sources generating heat due to friction: contact of rotary tool shoulder with the workpiece and high strain rate plastic work dissipation by the pin stirring. The tool is tungsten in their model, and the workpiece is 304L stainless steel. Here, in addition to the frictional heat, another source in the EA-FSW is the heat generated due to the Joule effect. These heat sources are formulated as below.

The main source of heat is on the upper part of the workpiece. If all the shearing work at the interface is converted into friction heat, the average heat input per unit area and time becomes

$$q_{0F} = 4\pi^2 \mu P N R^3 / 3 \tag{9}$$

where q_{0F} is the net power, μ is the friction coefficient, P is the pressure, N is the rotational speed, and R is the tool shoulder surface radius.

The heat generated, in this case, is directly proportional to the friction coefficient which changes with the temperature. Thus, at high temperatures, the heat generation efficiency decreases due to changes in the material’s physical properties.

At the lower part of the workpiece, the main heat generation source is the plastic deformation due to pin stirring, which is given by the following equation:

$$q_{0P}(t, x, y, z) = \eta s_{ij} \dot{\epsilon}_{ij}^P \quad (10)$$

where s_{ij} is the deviatoric stress tensor, $\dot{\epsilon}_{ij}^P$ is the incremental plastic strain rate tensor, and η is the energy input coefficient.

The heat generated by the rotary friction and plastic deformation was applied as a heat flux on the tool shoulder and pin. The heat generated due to rotary friction could be calculated from Equation (9). However, due to the difficulty in calculating the heat generated using Equation (10), total energy input was used to calculate this fraction of heat generation. Tool pin experiences a high wear rate due to the lower temperature of the lower part of the workpiece. The temperature is raised in this zone when the electrical current is applied. The following equation could calculate this heat generation:

$$q_{0R} = I^2 R t \quad (11)$$

where I is the current intensity, R is the electrical resistance of the tool/workpiece interface or contact resistance, and t is the current passing time.

8. Challenges and Outlooks

Similar to all joining processes, EA-FSW has limitations and drawbacks. One of the main weaknesses of this process is that it needs additional arrangements to carry it out. These additional arrangements increase the process expenses. EA-FSW needs cooling and insulation systems for safety and to decrease the tool temperature for excessive current. There is a wide variety of structures that EA-FSW can consider, and the available literature is not enough to conclude on the drawbacks and benefits of this process. One key point that should be considered deeply is the thermal history during the process. On the other hand, how can the electrical current improve friction stir spot welding? The mechanism of selecting the electrical current is not considered. The amount of electrical current and electrical current passing period through the metals can produce different temperatures.

FSW welds hard metals and dissimilar joints such as aluminum-copper or polymer-metal joints, and it is unclear whether these joints are feasible to weld by EA-FSW. Moreover, it is unclear whether the EA-FSW has benefits compared with FSW or not. The fracture mechanism and microstructure have not been considered deeply. Wear of the joining tool during EA-FSW is not considered, and the only literature just mentioned statistical data on this topic. The main point that can be considered in the future would be the simulation of this process for different materials and conditions to understand how extra heat made by electrical current could help the final joint properties.

Author Contributions: Conceptualization, H.A.D. and M.S.; formal analysis, H.A.D., J.W.G.G. and M.S.; investigation, H.A.D., J.W.G.G. and M.S.; resources, H.A.D., J.W.G.G. and M.S.; data curation, H.A.D., J.W.G.G. and M.S.; writing—original draft preparation, H.A.D., J.W.G.G. and M.S.; writing—review and editing, H.A.D., J.W.G.G. and M.S.; visualization, H.A.D., J.W.G.G. and M.S.; supervision, H.A.D.; project administration, H.A.D.; All authors have read and agreed to the published version of the manuscript.

Funding: This research received no external funding.

Institutional Review Board Statement: Not applicable.

Informed Consent Statement: Not applicable.

Data Availability Statement: Not applicable.

Conflicts of Interest: The authors declare no conflict of interest.

References

1. Derazkola, H.A.; Khodabakhshi, F. Underwater submerged dissimilar friction-stir welding of AA5083 aluminum alloy and A441 AISI steel. *Int. J. Adv. Manuf. Technol.* **2019**, *102*, 4383–4395. [[CrossRef](#)]
2. Khalaf, H.I.; Al-Sabur, R.; Demiral, M.; Tomków, J.; Łabanowski, J.; Abdullah, M.E.; Aghajani Derazkola, H. The Effects of Pin Profile on HDPE Thermomechanical Phenomena during FSW. *Polymers* **2022**, *14*, 4632. [[CrossRef](#)]
3. Mahto, R.P.; Gupta, C.; Kinjawadekar, M.; Meena, A.; Pal, S.K. Weldability of AA6061-T6 and AISI 304 by underwater friction stir welding. *J. Manuf. Process.* **2019**, *38*, 370–386. [[CrossRef](#)]
4. Mugada, K.K.; Adepu, K. Influence of ridges shoulder with polygonal pins on material flow and friction stir weld characteristics of 6082 aluminum alloy. *J. Manuf. Process.* **2018**, *32*, 625–634. [[CrossRef](#)]
5. Derazkola, H.A.; MohammadiAbokheili, R.; Kordani, N.; Garcia, E.; Murillo-Marrodán, A. Evaluation of nanocomposite structure printed by solid-state additive manufacturing. *CIRP J. Manuf. Sci. Technol.* **2022**, *37*, 174–184. [[CrossRef](#)]
6. Inaniwa, S.; Kurabe, Y.; Miyashita, Y.; Hori, H. Application of friction stir welding for several plastic materials. In Proceedings of the 1st International Joint Symposium on Joining and Welding, Osaka, Japan, 6–8 November 2013; Woodhead Publishing, 2013; pp. 137–142, ISBN 978-1-78242-163-4.
7. Bheekya Naik, R.; Venkateswara Reddy, K.; Madhusudhan Reddy, G.; Arockia Kumar, R. Microstructure, mechanical and wear properties of friction stir processed Cu-1.0%Cr alloys. *Fusion Eng. Des.* **2021**, *164*, 112202. [[CrossRef](#)]
8. Aghajani Derazkola, H.; Simchi, A. Processing and characterizations of polycarbonate/alumina nanocomposites by additive powder fed friction stir processing. *Thin-Walled Struct.* **2020**, *157*, 107086. [[CrossRef](#)]
9. Kang, S.H.; Vasudevan, M.; Noh, S.; Jin, H.J.; Jang, J.; Kim, T.K. Friction stir welding of F/M ODS steel plug and F/M steel tube. *Fusion Eng. Des.* **2016**, *109–111*, 182–185. [[CrossRef](#)]
10. Tanigawa, H.; Ozawa, K.; Morisada, Y.; Noh, S.; Fujii, H. Modification of vacuum plasma sprayed tungsten coating on reduced activation ferritic/martensitic steels by friction stir processing. *Fusion Eng. Des.* **2015**, *98–99*, 2080–2084. [[CrossRef](#)]
11. Khalaf, H.I.; Al-sabur, R.; Abdullah, M.E.; Kubit, A.; Derazkola, H.A. Effects of Underwater Friction Stir Welding Heat Generation on Residual Stress of AA6068-T6 Aluminum Alloy. *Materials* **2022**, *15*, 2223. [[CrossRef](#)]
12. Aghajani Derazkola, H.; Kordani, N.; Aghajani Derazkola, H. Effects of friction stir welding tool tilt angle on properties of Al-Mg-Si alloy T-joint. *CIRP J. Manuf. Sci. Technol.* **2021**, *33*, 264–276. [[CrossRef](#)]
13. Bokov, D.O.; Jawad, M.A.; Suksatan, W.; Abdullah, M.E.; Świerczyńska, A.; Fydrych, D.; Derazkola, H.A. Effect of pin shape on thermal history of aluminum-steel friction stir welded joint: Computational fluid dynamic modeling and validation. *Materials* **2021**, *14*, 7883. [[CrossRef](#)] [[PubMed](#)]
14. Liu, Z.Y.; Xiao, B.L.; Wang, W.G.; Ma, Z.Y. Analysis of carbon nanotube shortening and composite strengthening in carbon nanotube/aluminum composites fabricated by multi-pass friction stir processing. *Carbon* **2014**, *69*, 264–274. [[CrossRef](#)]
15. Liu, Z.Y.; Xiao, B.L.; Wang, W.G.; Ma, Z.Y. Developing high-performance aluminum matrix composites with directionally aligned carbon nanotubes by combining friction stir processing and subsequent rolling. *Carbon* **2013**, *62*, 35–42. [[CrossRef](#)]
16. Xu, X.; Zhang, C.; Derazkola, H.A.; Demiral, M.; Zain, A.M.; Khan, A. UFSW tool pin profile effects on properties of aluminium-steel joint. *Vacuum* **2021**, *192*, 110460. [[CrossRef](#)]
17. Liu, Z.Y.; Xiao, B.L.; Wang, W.G.; Ma, Z.Y. Singly dispersed carbon nanotube/aluminum composites fabricated by powder metallurgy combined with friction stir processing. *Carbon* **2012**, *50*, 1843–1852. [[CrossRef](#)]
18. Izadi, H.; Gerlich, A.P. Distribution and stability of carbon nanotubes during multi-pass friction stir processing of carbon nanotube/aluminum composites. *Carbon* **2012**, *50*, 4744–4749. [[CrossRef](#)]
19. Aghajani Derazkola, H.; García, E.; Eyvazian, A.; Aberoumand, M. Effects of rapid cooling on properties of aluminum-steel friction stir welded joint. *Materials* **2021**, *14*, 908. [[CrossRef](#)]
20. Campanelli, S.; Casalino, G.; Casavola, C.; Moramarco, V. Analysis and Comparison of Friction Stir Welding and Laser Assisted Friction Stir Welding of Aluminum Alloy. *Materials* **2013**, *6*, 5923–5941. [[CrossRef](#)]
21. Ruilin, L.; Diqui, H.; Luocheng, L.; Shaoyong, Y.; Kunyu, Y. A study of the temperature field during ultrasonic-assisted friction-stir welding. *Int. J. Adv. Manuf. Technol.* **2014**, *73*, 321–327. [[CrossRef](#)]
22. Derazkola, H.A.; Khodabakhshi, F. A novel fed friction-stir (FFS) technology for nanocomposite joining. *Sci. Technol. Weld. Join.* **2020**, *25*, 89–100. [[CrossRef](#)]
23. Padhy, G.K.; Wu, C.S.; Gao, S. Auxiliary energy assisted friction stir welding – Status review. *Sci. Technol. Weld. Join.* **2015**, *20*, 631–649. [[CrossRef](#)]
24. Luo, J.; Wang, X.J.; Wang, J.X. New technological methods and designs of stir head in resistance friction stir welding. *Sci. Technol. Weld. Join.* **2009**, *14*, 650–654. [[CrossRef](#)]
25. Saha, R.; Biswas, P. Current status and development of external energy-assisted friction stir welding processes: A review. *Weld. World* **2022**, *66*, 577–609. [[CrossRef](#)]
26. Pitschman, M.; Dolecki, J.W.; Johns, G.W.; Zhou, J.; Roth, J.T. Application of Electric Current in Friction Stir Welding. In Proceedings of the International Manufacturing Science and Engineering Conference, Erie, PA, USA, 12–15 October 2010; pp. 185–189.
27. Potluri, H.; Jones, J.J.; Mears, L. Comparison of Electrically-Assisted and Conventional Friction Stir Welding Processes by Feed Force and Torque. In Proceedings of the International Manufacturing Science and Engineering Conference, Madison, WI, USA, 10–14 June 2013.

28. Santos, T.G.; Miranda, R.M.; Vilaça, P. Friction stir welding assisted by electrical joule effect to overcome lack of penetration in aluminium alloys. *Key Eng. Mater.* **2014**, *611–612*, 763–772. [[CrossRef](#)]
29. Santos, T.G.; Miranda, R.M.; Vilaça, P. Friction Stir Welding assisted by electrical Joule effect. *J. Mater. Process. Technol.* **2014**, *214*, 2127–2133. [[CrossRef](#)]
30. Chen, S.; Zhang, H.; Jiang, X.; Yuan, T.; Han, Y.; Li, X. Mechanical properties of electric assisted friction stir welded 2219 aluminum alloy. *J. Manuf. Process.* **2019**, *44*, 197–206. [[CrossRef](#)]
31. Luo, J.; Chen, W.; Fu, G. Hybrid-heat effects on electrical-current aided friction stir welding of steel, and Al and Mg alloys. *J. Mater. Process. Technol.* **2014**, *214*, 3002–3012. [[CrossRef](#)]
32. Chen, S.; Wang, L.; Jiang, X.; Yuan, T.; Jiang, W.; Liu, Y. Microstructure and mechanical properties of AZ31B Mg alloy fabricated by friction stir welding with pulse current. *J. Manuf. Process.* **2021**, *71*, 317–328. [[CrossRef](#)]
33. Han, Y.; Jiang, X.; Chen, S.; Yuan, T.; Zhang, H.; Bai, Y.; Xiang, Y.; Li, X. Microstructure and mechanical properties of electrically assisted friction stir welded AZ31B alloy joints. *J. Manuf. Process.* **2019**, *43*, 26–34. [[CrossRef](#)]
34. Han, Y.; Chen, S.; Jiang, X.; Bai, Y.; Yuan, T.; Wang, X. Effect of microstructure, texture and deformation behavior on tensile properties of electrically assisted friction stir welded Ti-6Al-4 V joints. *Mater. Charact.* **2021**, *176*, 111141. [[CrossRef](#)]
35. Jiang, X.; Han, Y.; Chen, S.; Bai, Y.; Yuan, T.; Wang, X. Microstructure and texture investigation on electrically assisted friction stir welded titanium alloy. *Mater. Sci. Technol.* **2020**, *36*, 1628–1638. [[CrossRef](#)]
36. Das Chowdhury, I.; Sengupta, K.; Singh, D.K.; Roy, S.; Ghosal, S.; Mondal, A.K.; Sengupta, U. Study of mechanical properties of mild steel joint made by electrically assisted friction stir welding using DC and AC. *Mater. Today Proc.* **2021**, *44*, 3959–3966. [[CrossRef](#)]
37. Sengupta, K.; Kr Singh, D.; Mondal, A.K.; Bose, D.; Ghosh, B. Analysis of mechanical property of electrically assisted friction stir welding to enhance the efficiency of joints. *Mater. Today Proc.* **2021**, *38*, 2263–2270. [[CrossRef](#)]
38. Sengupta, K.; Singh, D.K.; Mondal, A.K.; Bose, D.; Patra, D.; Dhar, A. Characterization of tool wear in similar and dissimilar joints of MS and SS using EAFSW. *Mater. Today Proc.* **2021**, *44*, 3967–3975. [[CrossRef](#)]
39. Sengupta, K.; Chowdhury, I.; Banerjee, A.; Mondal, A.K.; Bose, D. Analysis of suitability of WC tool for joining Inconel 601 alloy by electric assisted friction stir welding. *Mater. Today Proc.* **2022**, *60*, 2093–2098. [[CrossRef](#)]
40. Xiaoqing, J.; Yongyong, L.; Tao, Y.; Shujun, C.; Lei, W.; Wang, J. Enhanced mechanical properties of dissimilar Al and Mg alloys fabricated by pulse current assisted friction stir welding. *J. Manuf. Process.* **2022**, *76*, 123–137. [[CrossRef](#)]
41. Shaffer, D.; Grimm, T.J.; Ragai, I.; Roth, J. Utilization of XSYTIN-1 Tool in Electrically-Assisted Friction Stir Welding of Dissimilar Metals - Al 6061-T651 to Mild Steel. *Adv. Mater. Res.* **2019**, *1152*, 31–41. [[CrossRef](#)]
42. Chen, K.; Liu, X.; Ni, J. Electrically Assisted Friction Stir Spot Welding of Aluminum Alloy to Advanced High Strength Steel. In Proceedings of the International Manufacturing Science and Engineering Conference, Los Angeles, CA, USA, 4–8 June 2017.
43. Li, M.; Xiong, X.; Ji, S.; Hu, W.; Yue, Y. Achieving high-quality metal to polymer-matrix composites joint via top-thermic solid-state lap joining. *Compos. Part B Eng.* **2021**, *219*, 108941. [[CrossRef](#)]
44. Aghajani Derazkola, H.; Kordani, N.; Mohammadi Abokheili, R. Investigation of joining mechanism of electrical-assist friction stir joining between polyethylene (PE) and 316 stainless steel. *Arch. Civ. Mech. Eng.* **2022**, *22*, 199. [[CrossRef](#)]
45. Sengupta, K.; Mondal, A.K.; Bose, D.; Singh, D.K. Fundamentals of Electric Resistance Friction Stir Welding of Metals: A Review. In Proceedings of the 2020 IEEE 1st International Conference for Convergence in Engineering (ICCE), Kolkata, India, 5–6 September 2020; pp. 32–37.
46. Memon, S.; Fydrych, D.; Fernandez, A.C.; Derazkola, H.A.; Derazkola, H.A. Effects of fsw tool plunge depth on properties of an al-mg-si alloy t-joint: Thermomechanical modeling and experimental evaluation. *Materials* **2021**, *14*, 4754. [[CrossRef](#)] [[PubMed](#)]
47. Yan, F.; Zhang, Y.; Fu, X.; Li, Q.; Gao, J. A new calculating method of frictional heat and its application during friction stir welding. *Appl. Therm. Eng.* **2019**, *153*, 250–263. [[CrossRef](#)]
48. Liu, X.; Lan, S.; Ni, J. Electrically assisted friction stir welding for joining Al 6061 to TRIP 780 steel. *J. Mater. Process. Technol.* **2015**, *219*, 112–123. [[CrossRef](#)]
49. Aghajani Derazkola, H.; Garcia, E.; Elyasi, M. Underwater friction stir welding of PC: Experimental study and thermo-mechanical modelling. *J. Manuf. Process.* **2021**, *65*, 161–173. [[CrossRef](#)]
50. Khodabakhshi, F.; Derazkola, H.A.; Gerlich, A.P. Monte Carlo simulation of grain refinement during friction stir processing. *J. Mater. Sci.* **2020**, *55*, 13438–13456. [[CrossRef](#)]
51. Long, X.; Khanna, S.K. Modelling of electrically enhanced friction stir welding process using finite element method. *Sci. Technol. Weld. Join.* **2005**, *10*, 482–487. [[CrossRef](#)]

Disclaimer/Publisher’s Note: The statements, opinions and data contained in all publications are solely those of the individual author(s) and contributor(s) and not of MDPI and/or the editor(s). MDPI and/or the editor(s) disclaim responsibility for any injury to people or property resulting from any ideas, methods, instructions or products referred to in the content.